Electronic Supplementary Material (ESI) for Catalysis Science & Technology.

Supporting Information

Carbon-coated nickel phosphide with enriched surface $Ni^{\delta+}$ sites enables an exceptional high productivity of 2-methyl furan from biomass upgrading

Xu Yang[a,b], Wu Liu[a,b], Shuyi Su[a,b], Jinfeng Li[a], Xiaoyang Wang [c,]*, Mengjie Lian[d], Lei Miao[c]*

[a] *School of Chemical Engineering and Light Industry, Guangdong University of Technology, Guangzhou, 510006, P. R. China*

[b] *Jieyang Branch of Chemistry and Chemical Engineering, Guangdong Laboratory (Rongjiang Laboratory), Jieyang, 515200, P. R. China*

[c] *Guangxi Key Laboratory for Relativity Astrophysics, State Key Laboratory of Featured Metal Materials and Life-cycle Safety for Composite Structures, School of Physical Science and Technology, Guangxi University, Nanning, 530004, P. R. China*

[d] *Guangxi Key Laboratory of Information Material, School of Material Science and Engineering, Guilin University of Electronic Technology, Guilin 541004, China*

* Corresponding author, Prof. X Yang, yangxu@gdut.edu.cn

*Corresponding author. Tel/Fax: +86 020-39322231. E-mail address: yangxu@gdut.edu.cn (X. Yang)

1. Experimental Section

Preparation of pure nickel nanoparticles (Ni NPs): Firstly, the Ni-MOFs were calcinated in the muffle oven at 500 °C in an air atmosphere for 4 h, and the resulting nickel oxide nanoparticles were denoted as NiO_x NPs. Next, the NiO_x NPs were reduced by hydrogen at 400 °C for 2 h, and cooled down to room temperature to obtain the pure nickel nanoparticles, Ni NPs.

Preparation of pure nickel phosphide nanoparticles (Ni_2P NPs): The as-obtained NiO_x NPs were phosphatized by gas-phosphidation as that of Ni_2P@C. The NiO_x NPs and NaH_2PO_2 were separately loaded on two quartz boats and heated to 300 °C for 1 h in Ar with a heating rate of 2 °C min^{-1}. After cooling to room temperature, the resulting products were washed with water and ethanol several times to remove the impurities and dried in a vacuum at 60 °C.

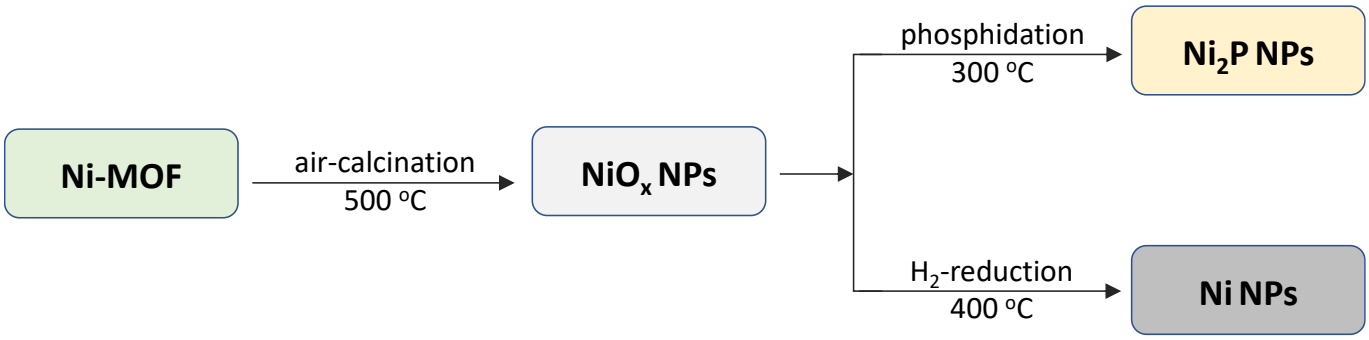

Scheme S1 Preparation procedure of pure Ni NPs and Ni_2P NPs without carbon coating.

2. Figures and Tables

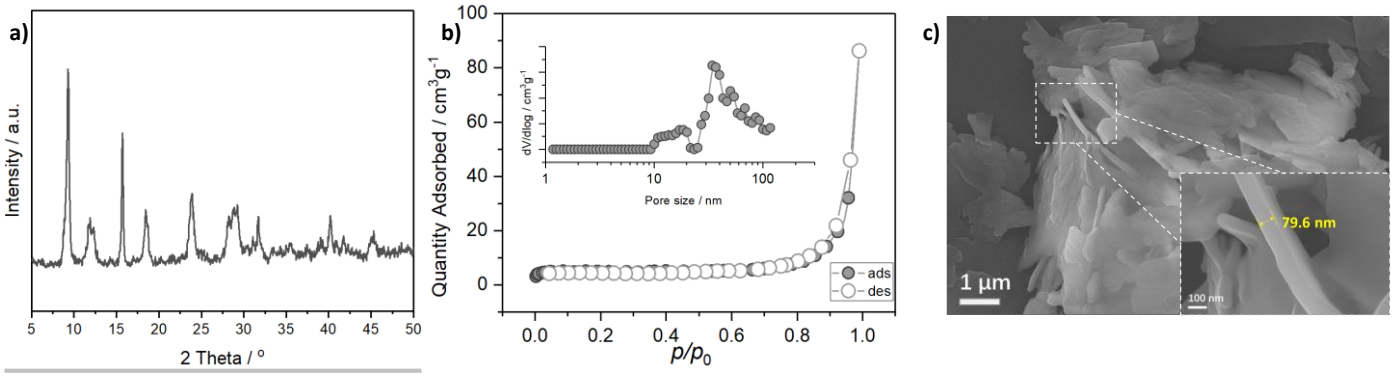

Figure S1 (a) XRD pattern, (b) nitrogen sorption with pore size distribution plot (inset) and (c) SEM images of the as-obtained Ni-MOF-ref. The Ni-MOF-ref stands for the reference sample prepared using the same method as the Ni-MOF, but without the addition of PVP. The Ni-MOF-ref showed almost identical XRD, nitrogen sorption profiles and morphology as those of Ni-MOF, suggesting the negligible effect of added PVP on their crystalline, porosity and morphology.

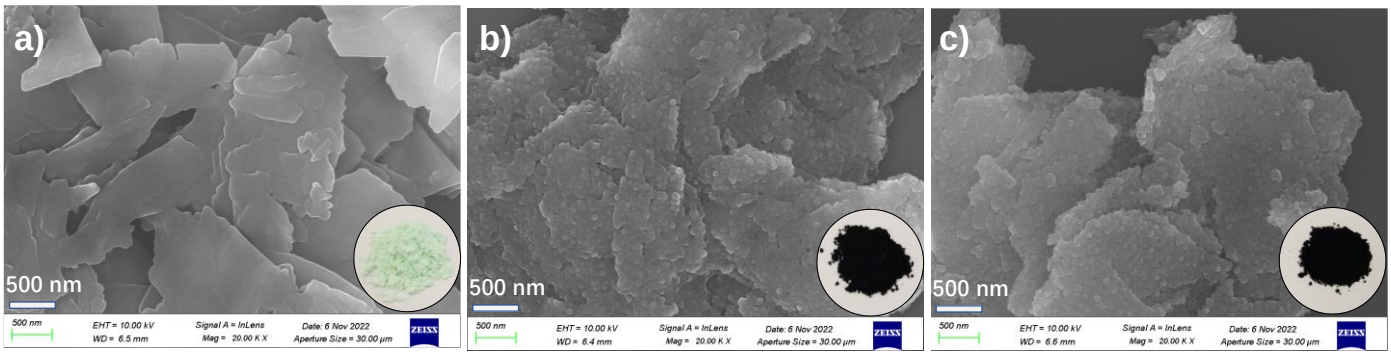

Figure S2 SEM images of the as-obtained Ni-MOF, Ni@C, and Ni_2P@C. Inset are their photographs of sample powder.

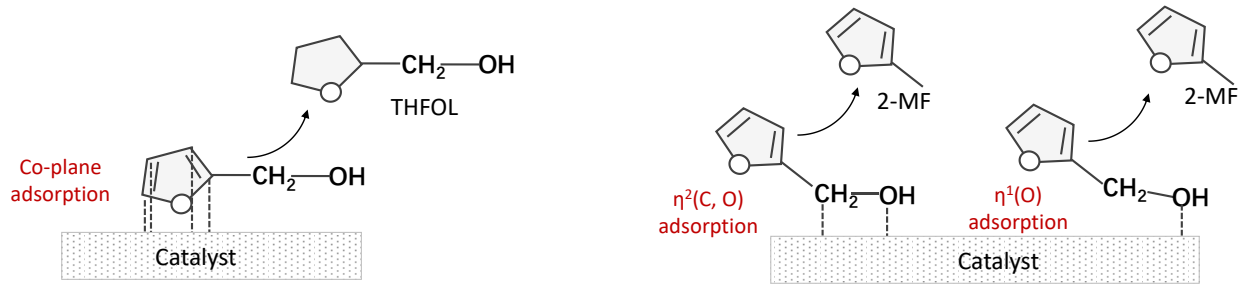

Figure S3 Various adsorption models of FOL on the catalyst lead to different products[1].

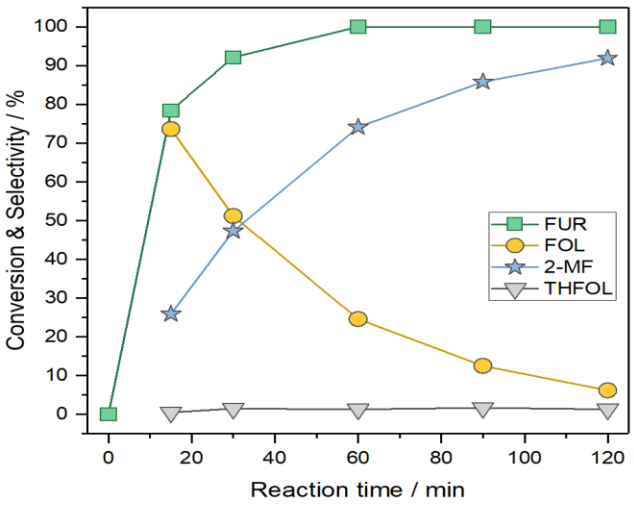

Figure S4 Catalytic performance over the Ni_2P@C using (e) FUR as substrate.

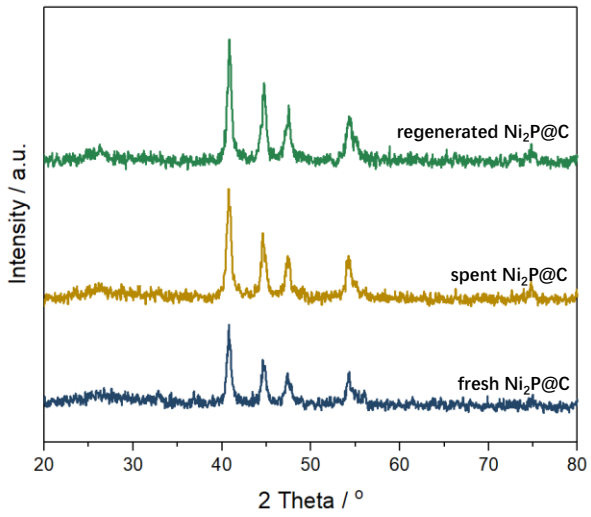

Figure S5 XRD pattern of fresh, spent and regenerated Ni_2P@C. Catalyst regeneration was calcinated in the nitrogen at 200 °C for 1 h.

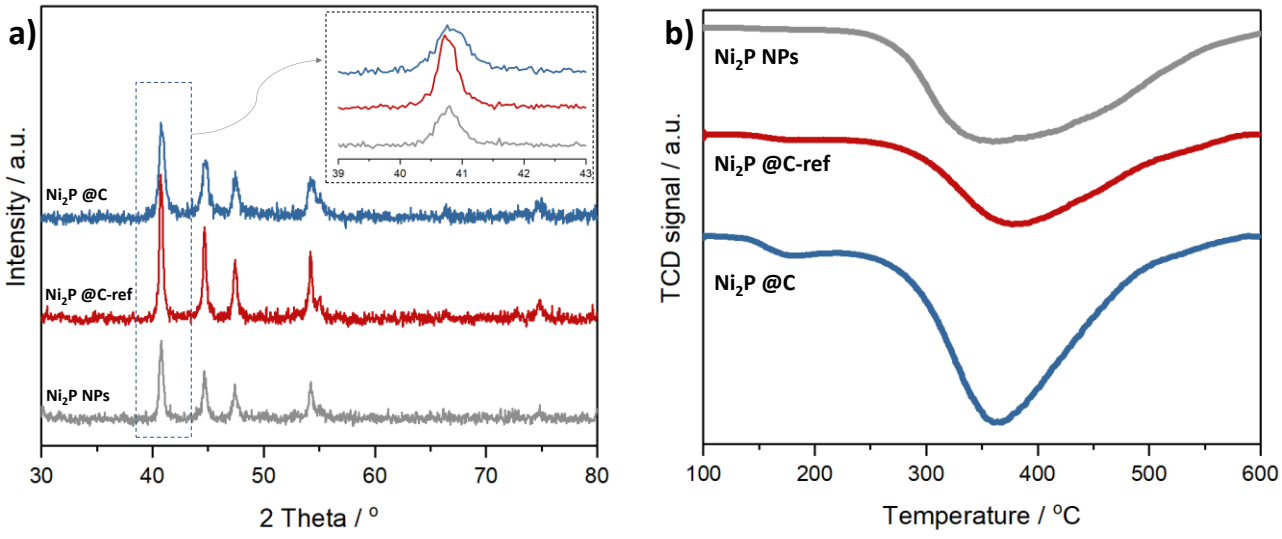

Figure S6 (a) XRD pattern of pure Ni_2P nanoparticles, Ni_2P@C and Ni_2P@C-ref, and inset was the magnified

region to see the broadening peak. The Ni_2P@C-ref refers to the sample prepared using the same procedure as the Ni_2P@C but without the addition of PVP. The pure Ni_2P nanoparticles (Ni_2P NPs) were prepared by calcination and phosphidation of Ni-MOF. **(b)** H_2-TPD profiles of various samples. These Ni_2P-based catalysts show a prominent desorption peak at a high-temperature range (>300 °C), indicating their capacity for hydrogen spillover[2, 3].

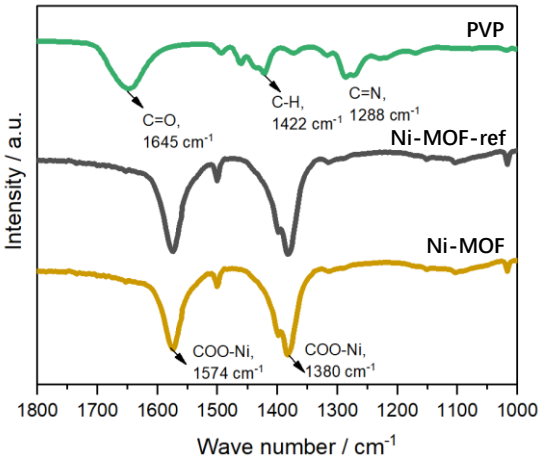

Figure S7 FTIR spectra of various samples. Two prominent peaks centered at ~1574 and ~1380 cm^{-1} are seen on the two nickel-based MOFs, corresponding to the asymmetric (ν_{as}) and symmetric (ν_s) stretching bands of the carboxylate group that coordinates with nickel[4]. Surprisingly, the characteristic peaks associated with the PVP, e.g., 1645 cm^{-1} of the C=O band, 1288-1268 cm^{-1} of the C-N band, etc., are conspicuously absent in the Ni-MOF spectrum, predicting the negligible presence of the PVP within the composite.

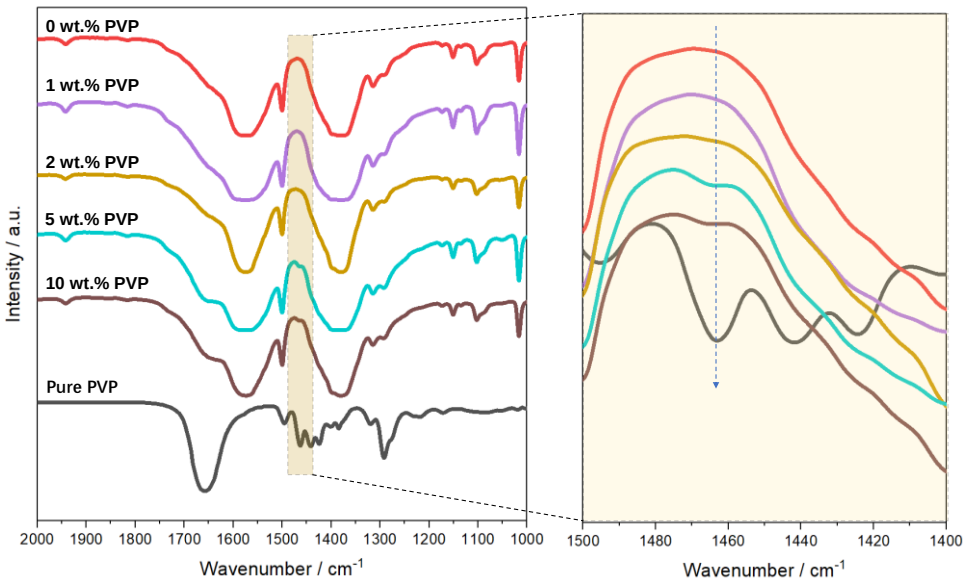

Figure S8 FTIR spectra of as-synthesized Ni-MOF-ref physically blended with various content of PVP. To investigate the detection limit of FTIR toward PVP content in the Ni-MOF-ref, we performed the FTIR spectrum for the Ni-MOF-ref that was physically blended with various content (wt.%) of PVP. As expected, when the content of PVP was dropped to 1 wt.%, the band at 1470~1460 cm^{-1} associated with the vibration of C-H bond in PVP disappeared[5]. This result demonstrates that the FTIR technique cannot confirm the low content of PVP as 1 wt.% in the Ni-MOF-ref.

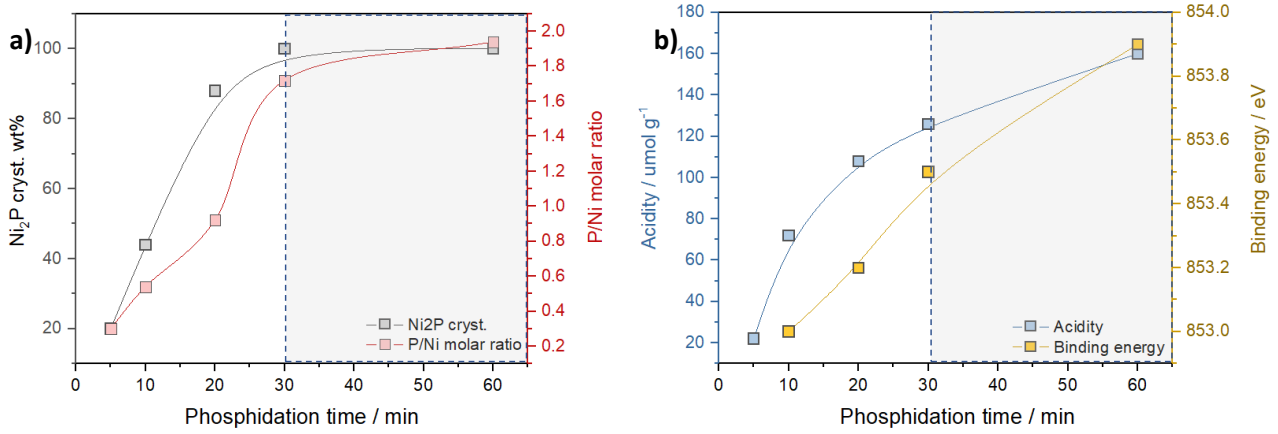

Figure S9 Evolution of structure specifications on the Ni_2P@C as a function of phosphidation time: (a) Ni_2P crystallite percentage and the molar ratio of P/Ni, (b) acidity and binding energy of Ni 2p. **Figure 8a-b** depicts the evolution of various structural properties (such as P/Ni ratio, acidity, etc.) as a function of phosphidation time. In the initial 30 min, the metallic Ni undergoes almost complete transformation into the Ni_2P phase. In accordance with this, the XPS-derived molar ratio of P/Ni increases linearly to ~1.7 and gradually reaches its maximum value during the extended phosphidation period. Interestingly, the binding energy of $Ni^{\delta+}$ continuously shifts towards higher values throughout the phosphidation process, accompanied by an increase in the acidity site capacity. These results elucidate that the initial formation of Ni_2P raises a strong Ni-P synergy, resulting in charge transfer from the Ni to P. Continued phosphidation strengthens this synergy, rendering these $Ni^{\delta+}$ species with more electron-deficiency and enhanced Lewis acidity. The decreased electron density of $Ni^{\delta+}$ species, as disclosed by Weber's group [14], weakens the C=C interaction, thereby

promoting the η^2(C, O) adsorption of the carbonyl group instead of the co-planar adsorption of the furan ring on the $Ni^{\delta+}$ sites. As a result, hydrogenolysis of FOL into 2-MF, rather than hydrogenation of furan ring into THFOL, preferentially occurs on the Ni_2P@C.

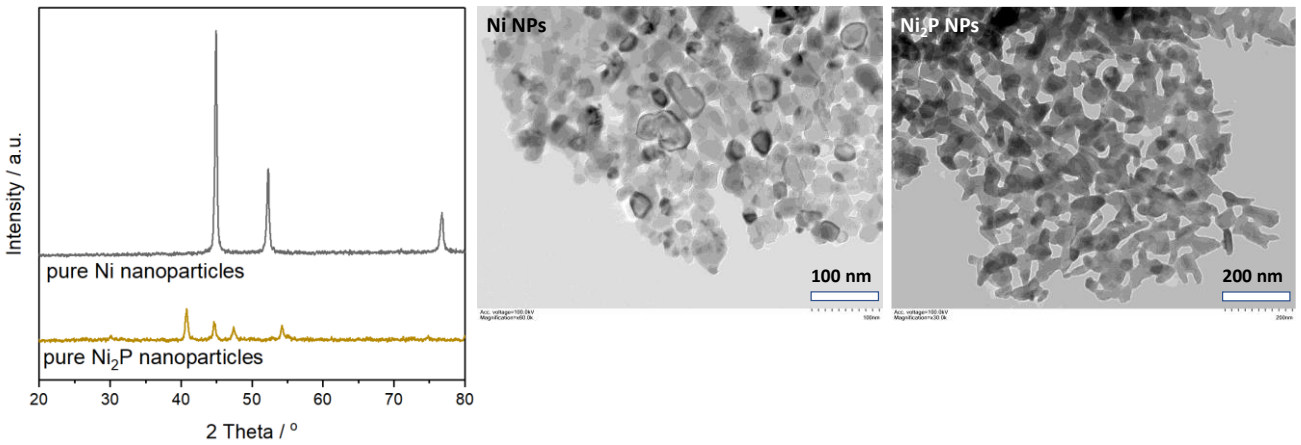

Figure S10 Structure characterizations of pure nickel and nickel phosphide nanoparticles.

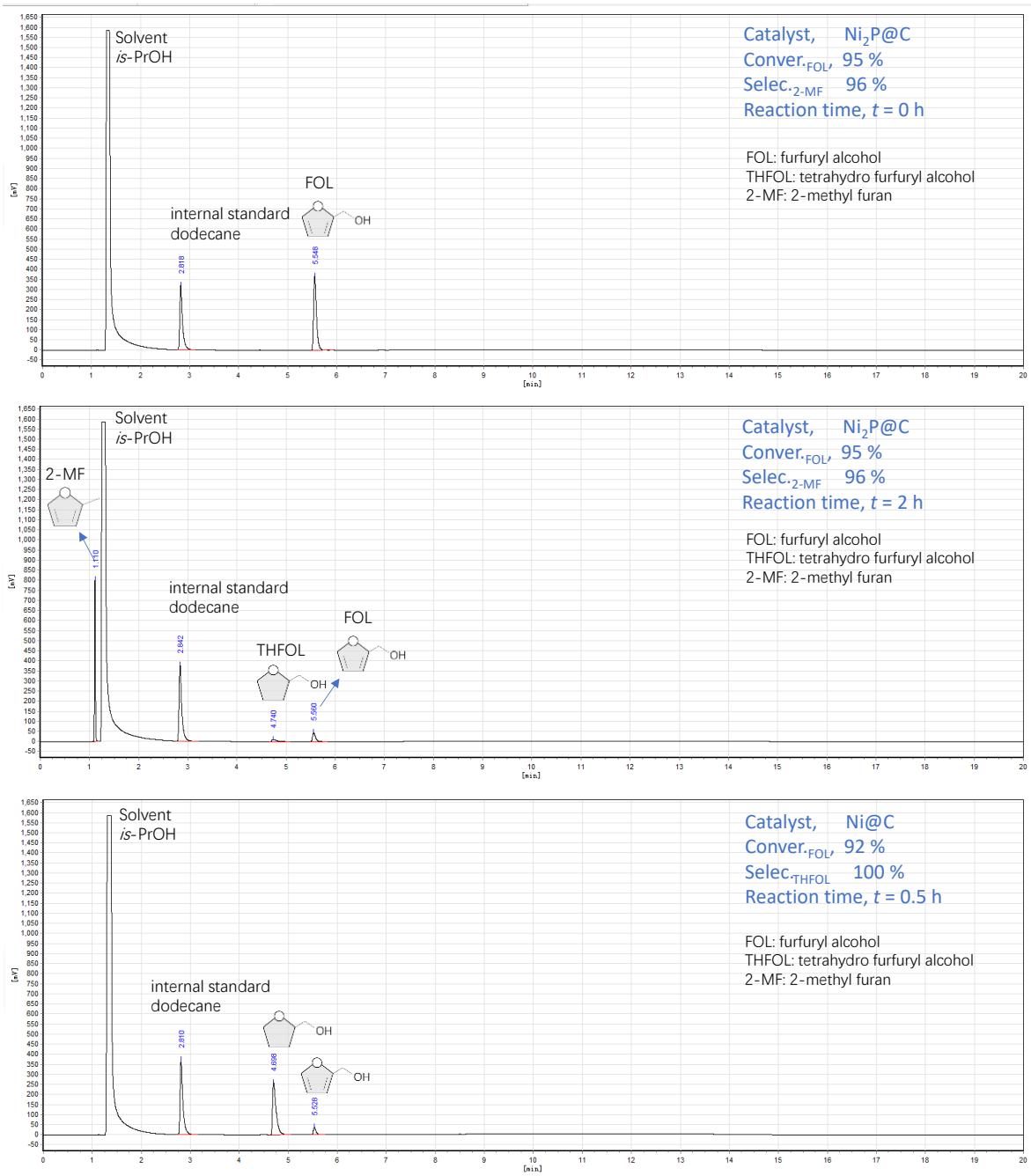

Figure S11 Representative gas chromatogram for several reaction runs.

Table S1 HDO of FOL over various catalysts. Reaction: 0.2 g of FOL, 50 mg of catalyst, 10 ml of isopropanol as the solvent, 0.2 g of octane as the internal standard, reacted at 120 ^{o}C and 2 MPa for 2 h.

Entry	**Catalyst**	**Conver.$_{FOL}$ / %**	**Selec.$_{2\text{-}MF}$ / %**	**Selec.$_{THFOL}$ / %**
1	none	< 0.1	n. a.	n. a.
2	Ni-MOF	< 0.1	n. a.	n. a.
3 [a]	Ni@C-ref	21	<1	>99
4 [a]	Ni@C	>99	1	99
5	Ni_2P@C-ref	49	88	12
6	Ni_2P@C	92	95	5
7[a]	pure Ni NPs	9	<1	>99
8	pure Ni_2P NPs	60	94	6

[a] 30 min of reaction period.

Table S2 HDO of FUR/FOL to produce 2-MF over various non-noble metal catalysts reported in the literature.

Catalyst	**Temp. / °C**	**p_{H2} / Mpa**	**Time / h**	**Conver. / %**	**Selec. / %**	**Rate / $g_{MF}g_{Cata}^{-1}\cdot h^{-1}$**	**Refs**
NiMo IMC/Al_2O_3	200	0.1	4	100	90	2.07	[6]
Ni_2P-1.00-300	240	1.5	4	100	91	1.32	[7]
NiCuAl	200	0.5	2	100	41	1.03	[8]
$Cu_1Re_{0.14}$/γ-Al_2O_3	200	2	6	100	86	0.72	[9]
Ni_2P_0.5	240	2	4	100	83	1.20	[10]
5/5% Cu/Ni	230	4	2	96	61	1.70	[11]
Ni_1Zn_3-MMO	200	3	6	100	95	0.92	[12]
α-MoC	150	3	6	96	90	1.12	[13]
10%Cu-10%Ni/TiO_2	200	-	-	100	84.5	0.63	[14]
MoP/SiO_2	120	1	-	100	96.3	0.25	[15]
Co/$CoAl_2O_4$	150	1.5	5	100	97.2	1.66	[16]
Co/SiO_2	180	1	-	94.8	88.2	0.71	[17]
Cu_3-Mo_1/CoO_x	180	2	4	99.9	92.04	0.64	[18]
20wt%Co-CoO_x/AC	120	2.5	5	100	88.2	1.51	[19]
5Cu3Re/Al_2O_3	220	-	4	100	94	1.00	[20]
Ni_2P@C	120	2	2	92	95	1.7	Thin work
Ni_2P@C	100	2	6	84	96	0.54	This work

Table S3 HDO of FOL over various catalysts. Reaction: 0.2 g of FOL, 50 mg of catalyst, 10 ml solvent, 0.2 g of octane as the internal standard, reacted at 120 °C and 2 MPa of gaseous pressure for 2 h.

Entry	Catalyst	Solvent	Gas charged	Conver.$_{FOL}$ / %	Selec.$_{2\text{-}MF}$ / %	Selec.$_{THFOL}$ / %
1	Ni_2P@C	iso-PrOH	H_2, 2 Mpa	92	94	6
2	Ni_2P@C	iso-PrOH	N_2, 2 Mpa	4	n. a.	n. a.
3	Ni_2P@C	hexane	H_2, 2 Mpa	44	83	31

Table S4 Structure specifications of Ni_2P based catalysts with various particle size or phosphidation time.

Catalyst	$T_{phosphi.}$ / min	[a] $D_{Cryst.}$ / nm	[b] S_{metal} / m^2g^{-1}	[c] $X_{Ni\delta+}$ / %	[d] $S_{Ni\delta+}$ / m^2g^{-1}
Ni_2P NPs	60	21.6 (22.5)	44	46	16
Ni_2P@C-ref	60	28.5 (30.1)	33	48	22
Ni_2P@C	60	13.2 (14.5)	72	45	32
Ni_2P@C	30	13.2	72	38	27
Ni_2P@C	20	13.1	72	25	18
Ni_2P@C	10	13.2	72	14	10

[a] Crystallite size ($D_{Cryst.}$) was calculated using the Scherrer equation, and the corresponding values measured from the TEM images were given in the bracket; [b] Metal surface area (S_{metal}) was measured using the equation, $S = \frac{6000}{\rho \times d}$, where the ρ is the density of Ni_2P, 6.31 g cm^{-3}, and d is the crystallite size of Ni_2P calculated from the HRTEM images[21]; [c] percentage of surface $Ni^{\delta+}$ species ($X_{Ni\delta+}$) was determined from the XPS derived atomic ratio; [d] surface $Ni^{\delta+}$ density ($S_{Ni\delta+}$) was calculated using the equation, $S_{Ni\delta+}=S_{metal}\times X_{Ni\delta+}$.

Reference

1. X. Lan, R. Pestman, E. J. M. Hensen and T. Weber, *Journal of Catalysis*, 2021, **403**, 181-193.
2. A. Infantes-Molina, E. Gralberg, J. A. Cecilia, E. Finocchio and E. Rodríguez-Castellón, *Catalysis Science & Technology*, 2015, **5**, 3403-3415.
3. S.-K. Wu, P.-C. Lai, Y.-C. Lin, H.-P. Wan, H.-T. Lee and Y.-H. Chang, *ACS Sustainable Chemistry & Engineering*, 2013, **1**, 349-358.
4. Z. Tong, X. Li, J. Dong, R. Gao, Q. Deng, J. Wang, Z. Zeng, J.-J. Zou and S. Deng, *ACS Catalysis*, 2021, **11**, 6406-6415.
5. A. Massoud, S. Challan and N. Maziad, *Journal of Macromolecular Science, Part A*, 2021, **58**, 408-418.
6. S. Fujita, K. Nakajima, J. Yamasaki, T. Mizugaki, K. Jitsukawa and T. Mitsudome, *ACS Catalysis*, 2020, **10**, 4261-4267.
7. Y. Wang, X. Feng, S. Yang, L. Xiao and W. Wu, *Journal of Nanoparticle Research*, 2020, **22**, 67.
8. M. Kalong, P. Hongmanorom, S. Ratchahat, W. Koo-amornpattana, K. Faungnawakij, S. Assabumrungrat, A. Srifa and S. Kawi, *Fuel Processing Technology*, 2021, **214**, 106721.
9. J. Chuseang, R. Nakwachara, M. Kalong, S. Ratchahat, W. Koo-amornpattana, W. Klysubun, P. Khemthong, K. Faungnawakij, S. Assabumrungrat, V. Itthibenchapong and A. Srifa, *Sustainable Energy & Fuels*, 2021, **5**, 1379-1393.
10. Y. Wang, F. Liu, H. Han, L. Xiao and W. Wu, *ChemistrySelect*, 2018, **3**, 7926-7933.
11. T. Varila, E. Mäkelä, R. Kupila, H. Romar, T. Hu, R. Karinen, R. L. Puurunen and U. Lassi, *Catalysis Today*, 2021, **367**, 16-27.
12. X. Meng, L. Wang, L. Chen, M. Xu, N. Liu, J. Zhang, Y. Yang and M. Wei, *Journal of Catalysis*, 2020, **392**, 69-79.
13. Y. Deng, R. Gao, L. Lin, T. Liu, X.-D. Wen, S. Wang and D. Ma, *Journal of the American Chemical Society*, 2018, **140**, 14481-14489.
14. A. Jaswal, P. P. Singh, A. K. Kar, T. Mondal and R. Srivastava, *Fuel Processing Technology*, 2023, **245**, 107726.
15. Y. Yao, S. Liu, Y. Wang, T. Li, Z. Sun, Y.-Y. Liu and A. Wang, *Industrial & Engineering Chemistry Research*, 2023, **62**, 17681-17690.
16. Y. Li, Q. Shen, Y. Nian, F. Wang, X. Zhang, Z. Zhang, C. Bing, X. Fan and R. Ahishakiye, *Applied Catalysis B: Environmental*, 2024, **343**, 123529.
17. P. Liu, L. Sun, X. Jia, C. Zhang, W. Zhang, Y. Song, H. Wang and C. Li, *Molecular Catalysis*, 2020, **490**, 110951.
18. Y. An, Q. Wu, L. Niu, C. Zhang, Q. Liu, G. Bian and G. Bai, *Journal of Catalysis*, 2024, **429**, 115271.
19. Z. Zhang, Z. Zhang, X. Zhang, F. Wang, Z. Wang, Y. Li, X. Wang, R. Ahishakiye and X. Zhang, *Applied Surface Science*, 2023, **612**, 155871.
20. K. Zhou, J. Chen, Y. Cheng, Z. Chen, S. Kang, Z. Cai, Y. Xu and J. Wei, *ACS Sustainable Chemistry & Engineering*, 2020, **8**, 16624-16636.
21. G. Bergeret and P. Gallezot, in *Handbook of Heterogeneous Catalysis*, 2008, DOI: https://doi.org/10.1002/9783527610044.hetcat0038, pp. 738-765.